Journal of Materials Chemistry C

COMMUNICATION

Tuning photoionization mechanisms of molecular hybrid materials for EUV lithography applications

Lianjia Wu,[a] Martijn Tiekink,[a] Alexandre Giuliani,[b] Laurent Nahon[b] and Sonia Castellanos*[a]

Received 00th January 20xx,
Accepted 00th January 20xx

DOI: 10.1039/x0xx00000x

www.rsc.org/

The investigation of the photoionization processes of a series titanium oxo clusters evidenced that doping their organic shell with extended aromatic structures decreases their ionization energy and stabilises the resulting radical cations. Such tunability of their photochemistry arising from ligand exchange gives these hybrid compounds great potential as EUV photoresists.

Introduction

Hybrid inorganic-organic materials are catching the attention of scientists in the field of nanolithography in connection to the introduction of extreme ultraviolet (EUV) lithography.[1–4] This new technology is currently being implemented in the semiconductor industry in order to reach the sub-20 nm nodes required for the steady miniaturization of the components in integrated circuits. The much shorter wavelength (13.5 nm) employed by EUV lithography as compared to the ones used in traditional optical lithography (365, 248 or 193 nm light) allows to achieve the theoretical limit of 10 nm resolution in the optical projection. This drastic change in photon energy poses some challenges regarding state-of-the art photoresists, the photoactive materials that capture the optical pattern. A major concern is the low absorption of previous photoresists based on polymeric platforms at 13.5 nm. Another fundamental problem is that the correlation between the materials' reactivity towards EUV light and its molecular structure is not well established, given the complexity of the EUV-induced chemistry. In contrast to previous lithography, where a photoacid generator was selectively excited with UV light, the energy of EUV light surpasses by far the ionization potential of the photoresist material and leads to photoelectron emission, even from core atomic levels.[5] The photoemitted electrons scatter through the material and transfer their energy inducing further excitations and ionizations in the surrounding material.[2,6] Investigating at the molecular level the contribution of each of these processes to the formation of the final pattern is necessary in order to design new photoresist for EUV lithographic applications.

Metal oxo clusters (MOCs), as molecular hybrid materials with a core/shell-like configuration,[7–9] are promising EUV photoresists.[10,11] The inorganic metal oxo core gives MOCs enhanced EUV absorption,[12] and, as shown by other inorganic photoresists, can potentially yield better mechanical and chemical stability as well as etch resistance in the final patterns, as compared to conventional organic photoresist.[13,14] The molecular identity of MOCs, in turn, provides them with small and homogeneous size, which is expected to decrease the roughness of the patterns generated by EUV lithography. Recently, we proved that these types of materials can effectively work as EUV photoresists and that their EUV absorption and sensitivity can be modified by playing with the composition of the inorganic core.[10] In addition, because of their exchangeable organic shell,[15–17] MOCs have a remarkable synthetic versatility.

In this work, we took advantage of this last feature to tune the photon-induced reactivity of Ti-MOCs. The organic shells of Ti-based MOCs were "doped" with extended aromatic ligands to modify their highest occupied molecular orbital (HOMO) levels. By raising the energy of the HOMO, the ionization energy is lowered. It has been reported that EUV chemically amplified resists (CARs) with lower band gaps lead to the generation of more acids.[18] This is attributed to the formation of more electron-hole pairs during the scattering of photoelectrons emitted upon EUV absorption. Meanwhile, the resulting holes can be stabilized in the conjugated structure, which can be used as a channel to modulate hole-induced reactivity. Thus, by tuning the band gap of the materials and of the localization of their frontier orbitals, it is anticipated that their reactivity upon EUV exposure can be also tuned.

The photodissociation and photoionization of this series of Ti-based MOCs towards vacuum ultraviolet (VUV) radiation in

[a] *Advanced Research Center for Nanolithography, Science Park 110, 1098 XG Amsterdam, The Netherlands.*
[b] *SOLEIL, l'Orme des Merisiers, St Aubin, BP48, 91192 Gif sur Yvette Cedex, France.*
† Footnotes relating to the title and/or authors should appear here.
Electronic Supplementary Information (ESI) available: [details of any supplementary information available should be included here]. See DOI: 10.1039/x0xx00000x

the 7-12 eV energy range were investigated in the gas phase by mass spectrometry (MS). Although VUV-MS has been previously used to study metallic nanoparticles,[19–21] and very recently to study molecular tin-based oxo-cages,[22] to the best of our knowledge, this is the first time that this technique is used to investigate the photochemistry of well-defined metal oxo clusters. These experiments confirm the effect of the doping with aromatic ligands onto the ionization potential and stabilization of the ionized products. Furthermore, the study of the fragmentation processes induced by different photon energies can help to understand the chemistry triggered upon irradiation with higher energy photons, i.e. EUV photons. Specifically, it can give insights on the chemistry induced upon exposure to EUV light during the lithographic application, which mainly leads to the ionization of the material.

Experimental details

Materials

Reagents and solvents were purchased from Sigma-Aldrich and used as received without further purification.

Synthesis of Titanium Oxo Clusters

$Ti_8O_8(OOCtBu)_{16}$, Ti_8L_{16}, and 4-(9H-carbazol-9-yl)benzoic acid (CBA) were synthesized as previously reported.[23, 24, 25] The doping of the organic shell to synthesize $Ti_8L_{15}CB$, $Ti_8L_{15}BTC$ and $Ti_8L_{15}AC$ was performed through ligand exchange reactions. A solution of the aromatic carboxylic acid (1:1 mol ratio) in chloroform was added to a solution of Ti_8L_{16} in chloroform. The resulting yellow-green solution was stirred magnetically at room temperature for 1 hour. The solvent was evaporated under vacuum. Acetonitrile was added to the yellow solid. The suspension was filtered and washed with acetonitrile. The product was dried under vacuum and characterized with ^1H NMR and IR.

DFT Calculations

DFT calculations of titanium oxo clusters were performed using Gaussian 09.[26] The geometries of molecules were optimized using DFT calculations with the hybrid B3LYP functional and the 6-31G(d) basis set.[27,28] The pivalate ligands of the oxo clusters were simplified to acetate ligands to save computational efforts.

Ionization (APPI) and vacuum ultraviolet action spectroscopy based on mass spectrometry (VUV-MS)

Mass spectrometry was performed using a linear quadrupolar ion trap (Thermo Scientific LTQ XL) mass spectrometer using an atmospheric pressure photoionization (APPI) source, and coupled[29] to the DESIRS beamline at SOLEIL synchrotron radiation facility (France)[30], allowing to perform VUV action spectroscopy. In each experiment, 1 mg of analyte (titanium oxo cluster) was dissolved in 1 mL toluene and the solution was filtered before infusion into the APPI source at 4-6 µL/min flow rates. The molecule was ionized by the krypton discharge lamp of the ion source. The targeted precursor ions $[P]^+=[M-L]^+$ (where M=titanium oxo cluster and L=pivalate ligand) were selectively trapped and irradiated at a suitable photon dose that did not yield photoproducts above 10% relative yield and mass spectra were recorded in the 7-12 eV energy range. Photons were monochromatized by a 200 grooves/mm low dispersion grating and filtered from any high order light contribution using a Kr-filled gas filter. Fragmentation yield curves were normalized to the photon flux variations as measured by a Si photodiode (IRD AXUV).

Results and discussion

The MOCs investigated in this work consist of an octameric ring-shaped Ti oxo cluster connected through 8 bridging oxygen atoms and 16 bridging carboxylate ligands (8 in equatorial position and 8 in axial position with respect to the ring). In the pristine material the cluster features 16 pivalate ligands (Ti_8L_{16}, L = pivalate). Three carboxylate ligands based on extended aromatic systems were selected to dope the organic shell of the pivalate oxo cluster precursor (Scheme 1): 4-(9H-carbazol-9-yl)benzoate (CB)[24,25] and 2,2'-bithiophene-5-carboxylate (BTC) featuring electron-rich heteroaromatic structures, and 9-anthracenecarboxylate (AC). Each aromatic carboxylate ligand was incorporated in the titanium oxo pivalate cluster Ti_8L_{16} by means of ligand exchange to yield $Ti_8L_{15}CB$, $Ti_8L_{15}BTC$ and $Ti_8L_{15}AC$, respectively.

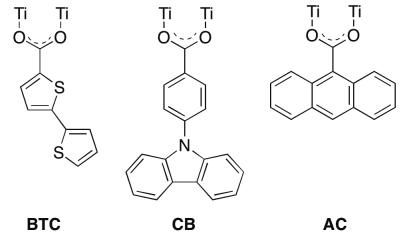

Scheme 1. Aromatic ligands introduced in the $Ti_8O_8Piv_{16}$ (Ti_8L_{16}) cluster by ligand exchange.

Figure 1 shows the calculated highest-occupied molecular orbital (HOMO) and lowest unoccupied molecular orbital (LUMO) energy and contour plot of the newly designed titanium oxo clusters when a doping ratio of 1:15 is used. To simplify the calculation, Ti oxo acetate clusters, rather than Ti oxo pivalate cluster were used. The two isomers resulting from the substitution of a pivalate ligand in the axial or the equatorial position have been considered. According to the DFT calculations, the HOMOs of the doped Ti-oxo clusters are located on the corresponding aromatic ligand and their eigenvalues are hence raised in comparison to the pristine cluster featuring only pivalate ligands, while their LUMOs remain on the ring structure of octameric Ti oxo core regardless of the presence of doping ligands. The calculated HOMO energy of Ti_8L_{16} is 7.37 eV, while this value increases by 1.5-2.2 eV for $Ti_8L_{15}BTC$, $Ti_8L_{15}CB$, and $Ti_8L_{15}AC$ (for calculations L=acetate), no matter which position (axial/equatorial) the new ligand exchanged (Table S1 in Supporting Information).

Journal of Materials Chemistry C

COMMUNICATION

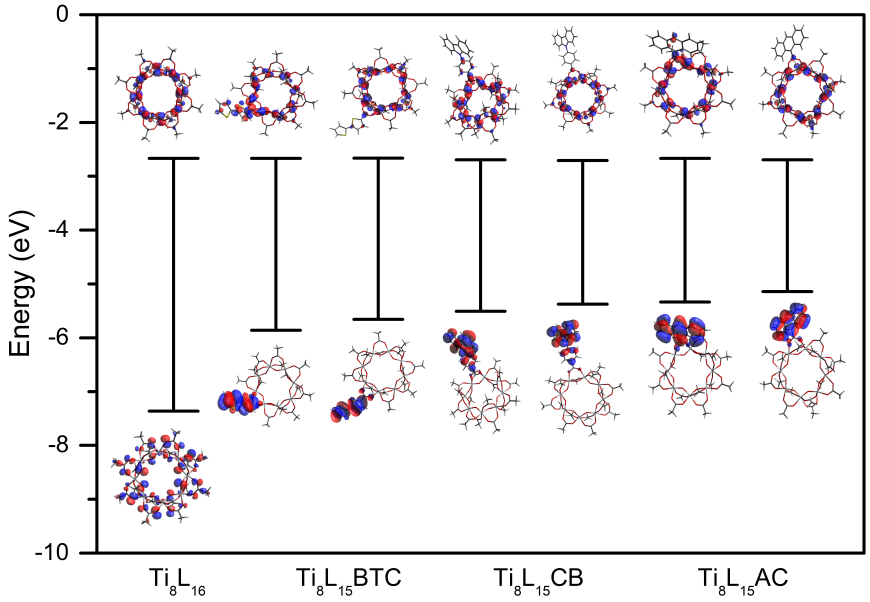

Figure 1. HOMO/LUMO energies and contour plots of the different Ti oxo clusters calculated with DFT using the hybrid B3LYP functional and the 6-31G(d) basis set.

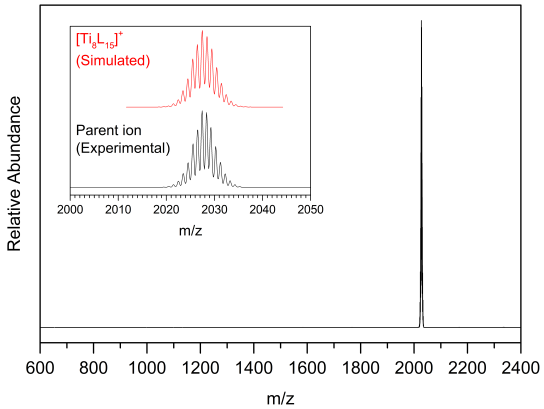

Figure 2 Mass spectrum of parent ion $[Ti_8L_{15}]^+$ and the simulated isotopic distribution.

APPI was used to generate the parent charged species from the initial neutral Ti oxo cluster molecules. In this technique, photons of 10.0 and 10.6 eV emitted by a krypton lamp are shone on the gas phase formed from the neutral molecules and the solvent (toluene). The latter gets ionized and reacts by charge exchange and/or proton transfer reactions with the neutral molecule. In the case of this series of Ti oxo clusters, APPI yielded the product corresponding to the loss of one pivalic acid, $[M\text{-}L]^+$. The resulting positively charged $[M\text{-}L]^+$ ion was selectively trapped as parent ion $[P]^+$ for VUV-MS experiments. The trapped parent ions were clearly identified as $[Ti_8L_{15}]^+$ with *m/z* 2027.5 (Figure 2), $[TiL_{14}BTC]^+$ with *m/z* 2135.4, $[Ti_8L_{14}CB]^+$ with *m/z* 2212.5, and $[TiL_{14}AC]^+$ with *m/z* 2147.5, respectively. In all cases the isotopic distribution perfectly matches the expected ratios for an octameric Ti-oxo cluster (Figures S9-S11 in Supporting Information).

Figure 3 displays the mass spectra of four trapped parent ions after VUV irradiation at 11 eV. For all four parent ions, the main photoproduct is identified as the product of pivalate photodissociation $[P\text{-}L]^+$: $[Ti_8L_{14}]^{+\bullet}$ (*m/z* 1926), $[Ti_8L_{13}BTC]^{+\bullet}$ (*m/z* 2035), $[Ti_8L_{13}CB]^{+\bullet}$ (*m/z* 2111), and $[Ti_8L_{13}AC]^{+\bullet}$ (*m/z* 2046), respectively. Note that the dissociation of the aromatic ligand from the doped parent to yield $[Ti_8L_{14}]^+$ was barely detected. Dicationic species $[Ti_8L_{14}BTC]^{2+\bullet}$ (*m/z* 1068), $[Ti_8L_{14}CB]^{2+\bullet}$ (*m/z* 1107), and $[TiL_{14}AC]^{2+\bullet}$ (*m/z* 1074) also appear in the spectra, although in much lower concentration. Interestingly, in the case of the non-doped Ti oxo cluster the ionized parent ion $[Ti_8L_{15}]^{2+\bullet}$ was not detected and only the dication $[Ti_8L_{14}]^{2+}$ (*m/z* 913) appears in the low mass region of the spectrum. Finally, dicationic species assigned to $[P\text{-}L]^{2+}$, $[Ti_8L_{13}BTC]^{2+}$ (*m/z* 966), $[Ti_8L_{13}CB]^{2+}$ (*m/z* 1005), and $[TiL_{13}AC]^{2+}$ (*m/z* 972) were present in much lower concentration.

In order to determine the photoionization energy threshold for this set of materials, the relative yield of dication formation

upon irradiation in the 7-12 eV energy range for the non-doped $[Ti_8L_{15}]^+$ and doped $[Ti_8L_{14}BTC]^+$, $[Ti_8L_{14}CB]^+$, and $[Ti_8L_{14}AC]^+$ was monitored (Figure 3). In the plots it can be observed that the dicationic species $[P\text{-}L]^{2+}$ is detected above 11 eV in all compounds. However, in the case of the doped clusters an extra curve can be plotted for the "clean" photoionization product $[P]^{2+}$, which is not accompanied by ligand dissociation. The ionization energy onsets for the doped compounds are 8.98 ± 0.07 eV for $[Ti_8L_{14}BTC]^+$, 8.42 ± 0.06 eV for $[Ti_8L_{14}CB]^+$ and 8.57 ± 0.03 eV for $[Ti_8L_{14}AC]^+$ (Figures S12-S15 in Supporting information).

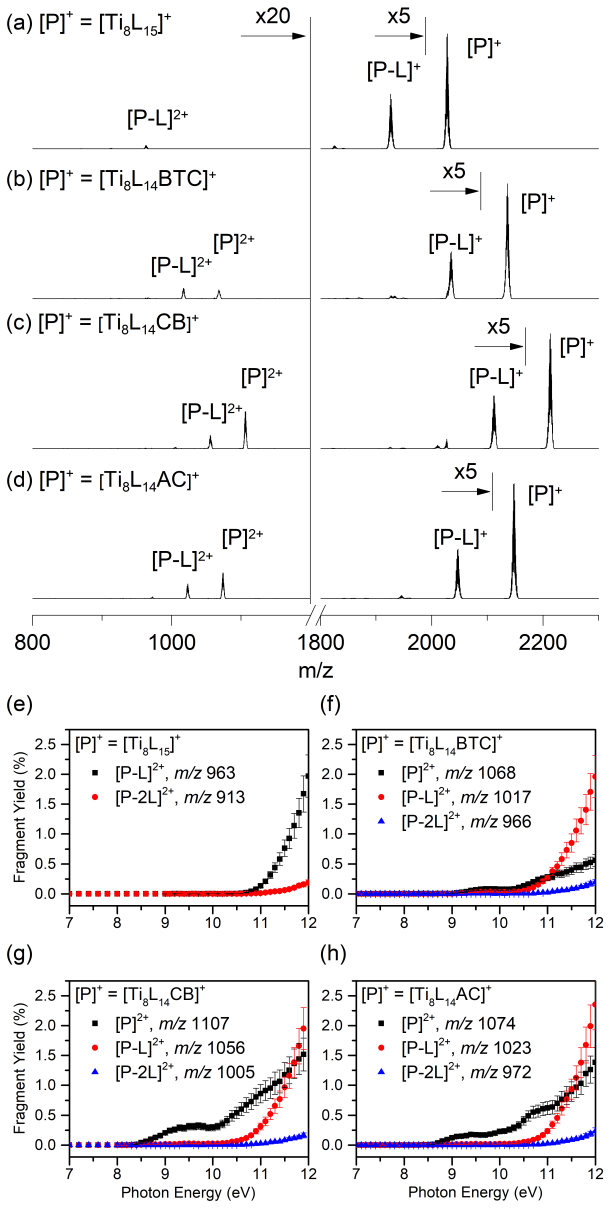

Figure 3. Mass spectra after photon activation at 11 eV (a-d) and fragment yields resulting from ionization of the parent ion $[P]^+$ as a function of photon energy (e-h).

These results indicate that in the case of the doped MOCs, which feature one aromatic ligand, the hole generated upon photoionization can be stabilized by the conjugated system. The non-doped parent compound, on the other hand, undergoes a dissociative ionization where a pivalate ligand is lost so that no $[TiL_{15}]^{2+\bullet}$ species is detected. The lower energy onsets for the photoionization of the doped clusters nicely follow the trends in their calculated HOMO values, where the presence of the aromatic ligands raise the HOMO levels by 1.5 to 2.2 eV. Yet, above 11 eV all compounds undergo a dissociative ionization. The photoreactions in the 7-12 eV energy range for the studied oxo clusters are thus summarized in Scheme 2.

(*a*) $h\nu$ >7 eV pivalate ligand dissociation $[P]^+ \rightarrow [P\text{-}L]^+$

$[Ti_8L_{15}]^+ + h\nu \rightarrow [Ti_8L_{14}]^{+\bullet} + L^\bullet$

$[Ti_8L_{14}L']^+ + h\nu \rightarrow [Ti_8L_{13}L']^{+\bullet} + L^\bullet$

(b) $h\nu$ >8.4-9 eV ionization of doped parent clusters $[P]^+ \rightarrow [P]^{2+}$

$[Ti_8L_{14}L']^+ + h\nu \rightarrow [Ti_8L_{14}L']^{2+\bullet} + e^-$

(c) $h\nu$ > 11 eV dissociative ionization $[P]^+ \rightarrow [P\text{-}L]^{2+}$

$[Ti_8L_{15}]^+ + h\nu \rightarrow [Ti_8L_{14}]^{2+} + e^- + L^\bullet$ (major)

$[Ti_8L_{15}]^+ + h\nu \rightarrow [Ti_8L_{13}]^{2+\bullet} + e^- + 2L^\bullet$ (minor)

$[Ti_8L_{14}L']^+ + h\nu \rightarrow [Ti_8L_{13}L']^{2+} + e^- + L^\bullet$ (major)

$[Ti_8L_{14}L']^+ + h\nu \rightarrow [Ti_8L_{12}L']^{2+\bullet} + e^- + 2L^\bullet$ (minor)

Scheme 2. Proposed photoexcitation reactions of the parent ions for the pristine Ti-MOC and the derived doped series.

The plot of the total fragmentation yield normalized by the photon flux as a function of photon energy gives the action spectra (equivalent to an absorption spectrum) of the four Ti oxo clusters. Photon absorption below 8.4 eV only yields the photodissociation of the pivalate ligands (Figure S16 in Supporting Information). Above, multiple decay paths contribute to the spectra: pivalate dissociation, net ionization, and dissociative ionization. A broad band can be observed at 8.5 eV for all compounds except for $[Ti_8L_{14}CB]^+$, where it appears as a smooth shoulder. At 10.5 eV, on the other hand, a sharp peak can be observed in all oxo clusters. This spectral feature could be related to a shape resonance in the dissociative ionization channel previously discussed.

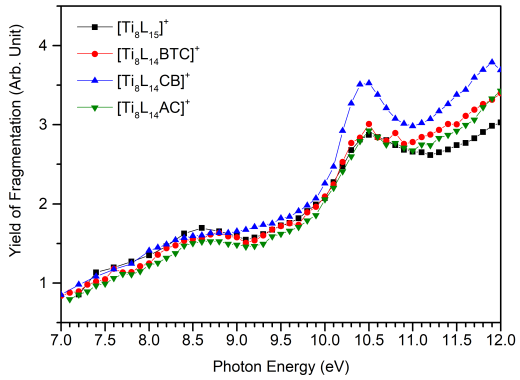

Figure 4. Action spectra of parent ions $[Ti_8L_{15}]^+$, $[Ti_8L_{14}BTC]^+$, $[Ti_8L_{14}CB]^+$, and $[Ti_8L_{14}AC]^+$. The estimated error is 16% (error bars are omitted for better visualization)

Conclusions

Doping the organic shell of Ti-based metal-oxo clusters with extended (hetero)aromatic structures proved to be a

straightforward method to decrease the photoionization threshold of this compound and to stabilize the ionized species, as evidenced by photofragmentation studies using VUV-MS. While the pristine $Ti_8O_8Piv_{16}$ MOC only undergoes dissociative ionization when irradiated with photon energies above 11 eV, the incorporation of phenylcarbazole-, bis-(thienyl)-, and anthracenyl-based carboxylate ligands in a 1:15 ratio opens an extra ionization channel located at ~2.0-2.5 eV lower energies. This different reactivity is attributed to the introduction of a new HOMO level that is mainly located in the aromatic doping ligand. This work highlights the great potential of MOCs as photoresists, since the synthetic versatility offered by ligand exchange reactions can be exploited to modify at will the reactivity of their ionized states. This feature makes them ideal molecular materials for the study of EUV induced photochemistry and will assist in the development of new EUV photoresist materials

Conflicts of interest

"There are no conflicts to declare".

Acknowledgements

Part of this work has been carried out at the Advanced Research Center for Nanolithography (ARCNL), a public-private partnership of the University of Amsterdam (UvA), the VU University Amsterdam (VU), the Netherlands Organisation for Scientific Research (NWO) and the semiconductor equipment manufacturer ASML. This work was partially supported by the Agence Nationale de la Recherche Scientifique, France, under project number ANR-08-BLAN-0065. The research leading to this result has been supported by the project CALIPSOplus under the Grant Agreement 730872 from the EU Framework Programme for Research and Innovation HORIZON 2020. We warmly thank the whole SOLEIL staff for running the facility under project 20171457.

References

1 N. Mark, K. Cho and K. Petrillo, *J. Photopolym. Sci. Technol.*, 2012, **25**, 87–94.
2 P. D. Ashby, D. L. Olynick, D. F. Ogletree and P. P. Naulleau, *Adv. Mater.*, 2015, **27**, 5813–5819.
3 L. Li, S. Chakrabarty, K. Spyrou, C. K. Ober and E. P. Giannelis, *Chem. Mater.*, 2015, **27**, 5027–5031.
4 L. Li, X. Liu, S. Pal, S. Wang, C. K. Ober and E. P. Giannelis, *Chem. Soc. Rev.*, 2017, **2**, 4855–4866.
5 K. D. Closser, D. F. Ogletree, P. Naulleau and D. Prendergast, *J. Chem. Phys.*, 2017, **146**, 164106.
6 A. Narasimhan, L. Wisehart, S. Grzeskowiak, L. E. Ocola, G. Denbeaux and R. L. Brainard, *J. Photopolym. Sci. Technol.*, 2017, **30**, 113–120.
7 U. Schubert, *Coord. Chem. Rev.*, 2017, **350**, 61–67.
8 U. Schubert, *Chem. Soc. Rev.*, 2011, **40**, 575–582.
9 C. Sanchez, K. J. Shea, S. Kitagawa and L. Rozes, *Chem. Soc. Rev.*, 2011, **40**, 1006–1030.
10 S. Castellanos, L. Wu, M. Baljozovic, G. Portale, D. Kazazis, M. Vockenhuber, Y. Ekinci and T. Jung, *Proc. SPIE*, 2018, **10583**, 105830A.
11 H. Xu, K. Sakai, K. Kasahara, V. Kosma, K. Yang, H. C. Herbol, J. Odent, P. Clancy, E. P. Giannelis and C. K. Ober, *Chem. Mater.*, 2018, **30**, 4124–4133.
12 R. Fallica, J. Haitjema, L. Wu, S. Castellanos, A. M. Brouwer and Y. Ekinci, *J. Micro/ Nanolithography, MEMS, MOEMS*, 2018, **17**, 23505.
13 M. Trikeriotis, M. Krysaki, Y. S. Chung, C. Ouyang, B. Cardineau, R. Brainard, C. K. Ober, E. P. Giannelis and K. Cho, *J. Photopolym. Sci. Technol.*, 2012, **25**, 583–586.
14 D. De Simone, M. Mao, M. Kocsis, P. De Schepper, F. Lazzarino, G. Vandenberghe, J. Stowers, S. Meyers, B. L. Clark, A. Grenville, V. Luong, F. Yamashita and D. Parnell, *Proc. SPIE*, 2016, **9776**, 97760B.
15 J. Kreutzer, M. Puchberger, C. Artner and U. Schubert, *Eur. J. Inorg. Chem.*, 2015, **2015**, 2145–2151.
16 P. Walther, M. Puchberger, F. R. Kogler, K. Schwarz and U. Schubert, *Phys. Chem. Chem. Phys.*, 2009, **11**, 3640–3647.
17 T. Frot, S. Cochet, G. Laurent, C. Sassoye, M. Popall, C. Sanchez and L. Rozes, *Eur. J. Inorg. Chem.*, 2010, **8**, 5650–5659.
18 S. Grzeskowiak, J. Kaminsky, S. Gibbons, M. Murphy, J. Chandonait, R. L. Brainard and G. Denbeaux, *Proc. SPIE*, 2018, **10586**, 105860D.
19 S. Daly, M. Krstic, A. Giuliani, R. Antoine, L. Nahon, A. Zavras and G. N. Khairallah, *Phys. Chem. Chem. Phys.*, 2015, **17**, 25772–25777.
20 C. S. Ah, H. S. Han, K. Kim and D. Jang, *J. Phys. Chem. C*, 2000, **104**, 8153–8159.
21 S. Daly, C. M. Choi, A. Zavras, M. Krstić, F. Chirot, T. U. Connell, S. J. Williams, P. S. Donnelly, R. Antoine, A. Giuliani, V. Bonačic-Koutecky, P. Dugourd and R. A. J. O'Hair, *J. Phys. Chem. C*, 2017, **121**, 10719–10727.
22 J. Haitjema, L. Wu, A. Giuliani, L. Nahon, S. Castellanos and A. M. Brouwer, *J. Photopolym. Sci. Technol.*, 2018, **31**, 243–247.
23 P. Piszczek, M. Richert, A. Grodzicki, T. Głowiak and A. Wojtczak, *Polyhedron*, 2005, **24**, 663–670.
24 S. H. Hsiao and Y. T. Chiu, *RSC Adv.*, 2015, **5**, 90941–90951.
25 G. S. Liou, S. H. Hsiao, N. K. Huang and Y. L. Yang, *Macromolecules*, 2006, **39**, 5337–5346.
26 M. J. Frisch et al., 2016, Gaussian, Inc., Wallingford CT.
27 Y. Fan, H. Li, R. Duan, H. Lu, J. Cao, G. Zou and Q. Jing, *Inorg. Chem.*, 2017, **56**, 12775–12782.
28 H.-T. Lv, H.-M. Li, G.-D. Zou, Y. Cui, Y. Huang and Y. Fan, *Dalt. Trans.*, 2018, **47**, 8158–8163.
29 A. R. Milosavljevic, C. Nicolas, J.-F. Gil, F. Canon, M. Refregiers, L. Nahon and A. Giuliani, *J. Synchrotron Radiat.*, 2012, **19**, 174–178.
30 L. Nahon, N. De Oliveira, G. A. Garcia, J. F. Gil, B. Pilette, O. Marcouillé, B. Lagarde and F. Polack, *J. Synchrotron Radiat.*, 2012, **19**, 508–520.